S/B-18

N93-27572

ADVANCED ACTUATORS FOR THE CONTROL OF LARGE SPACE STRUCTURES[1]

James Downer, Richard Hockney, Bruce Johnson, Kathleen Misovec

SatCon Technology Corporation
71 Rogers St.
Cambridge, MA

ABSTRACT

The objective of this research was to develop advanced six-degree-of-freedom actuators employing magnetic suspensions suitable for the control of structural vibrations in large space structures. The advanced actuators consist of a magnetically suspended mass that has three-degrees-of-freedom in both translation and rotation. The most promising of these actuators featured a rotating suspended mass providing structural control torques in a manner similar to a control moment gyro (CMG). These actuators employ large-angle-magnetic suspensions that allow gimballing of the suspended mass without mechanical gimbals. Design definitions and sizing algorithms for these CMG type as well as angular reaction mass actuators based on multi-degree-of-freedom magnetic suspensions were developed. The performance of these actuators was analytically compared with conventional reaction mass actuators for a simple space structure model.

INTRODUCTION

New spacecraft designs feature large structures characterized by low natural frequencies, lightly damped structural modes, and stringent pointing and vibration performance requirements. These large space structures (LSS) pose unique and difficult control problems. An important part of the solutions to these control problems in the development of actuators that allow the application of force and/or torque to the space structure.

The purpose of this research is to develop multi-directional actuators which employ magnetic suspensions and to assess their performance compared to conventional actuators. A baseline conventional linear reaction mass actuator is used in conjunction with a flexible structure model to size and evaluate the advanced actuators. The most promising actuator designs feature a rotating suspended mass providing control torques in a manner similar to a control moment gyro. Two small-stroke actuators were designed, one with a composite flywheel and the other with a steel flywheel. Several large-stroke actuators were designed which included both attraction force and Lorentz force designs. In addition, a large stroke actuator was designed which employs a superconducting coil.

The major advantages of these advanced actuators include high bandwidth compared to conventional CMG's and large momentum storage

[1] This work was performed under NASA grant NAS1-18426

capability, low mechanical noise, and multi-degree-of-freedom actuation compared to conventional linear reaction mass actuators. The combination of high bandwidth and large momentum storage allow these advanced actuators to be used in applications such as space robotic arms that have both slewing and vibration requirements. Because of their six-degree-of-freedom actuation characteristics, these advanced actuators were shown to be capable of replacing numerous linear reaction mass actuators.

LARGE SPACE STRUCTURE MODEL

Because a beam can be an appropriate simplified model for many different types of flexible structures, such as a robotic arm or a deployable truss structure, actuator performance was evaluated in conjunction with a finite element cantilevered beam model.

A beam of length 60 m with a lowest natural bending frequency of 1.15 rad/sec (0.184 Hz) was chosen for this analysis. A 247 kg mass with a moment of inertia of 20 kg m^2 was situated at the tip of this model (Misovec, 1987). Figure 1 is a plot of the first four mode shapes. The lowest mode in this plot has a large transverse deflection at the tip. As the excitation frequencies get higher, more energy is required to move the large tip mass, and the tip increasingly behaves like a pinned end.

Table 1. Lowest Four Natural Frequencies of 35 Element Model.

0.184 Hz
1.83 Hz
5.7 Hz
11.7 Hz

ACTUATOR SIZING AND PLACEMENT

Baseline Conventional Actuator

The SatCon actuators were sized to give comparable performance to that of a conventional linear reaction mass actuator. These conventional actuators produce control forces by accelerating the actuator mass. The conventional actuator is capable of producing forces in only one direction. The magnitude of the actuator force is limited by how fast the mass can be accelerated and by how far the mass is allowed to travel (the stroke).

The conventional actuator that will be used to size SatCon actuators has the characteristics listed in Table 2 (Davis, 1986). It is capable of producing a maximum of 30 N of force with an 11 kg reaction mass. The maximum stroke is 15 cm (7.5 cm in each direction). This stroke has a limiting effect on the force for excitation frequencies less 1 Hz. For the beam considered in this paper, only the forces produced to control the lowest mode are reduced because of stroke limitations. The maximum force production in this mode is 1.1 N. SatCon torque actuators were designed for equivalent performance with a force actuator which can produce 1.1 N to control a mode 1 excitation and 30 N of force for all the other excitation

modes.

Table 2. Conventional Actuator Characteristics.

Maximum Force Capability	=	30 N
Maximum Stroke	=	15 cm
Reaction Mass	=	11 Kg
Total Mass per Direction	=	20 Kg

Actuator Sizing Issues

Actuator Torque Sizing

Because the advanced actuators are capable of both force and torque production while the baseline conventional actuator is only capable of force production, a sizing relationship between force actuation and torque actuation was developed. Assuming that torque and force actuators act as dampers and remove equal amounts of power from a vibrating structure, an expression relating torque capability and force capability can be established (Misovec,1987):

$$\frac{\tau}{F} = \frac{x_{max}}{\theta_{max}} = l_b \qquad (1)$$

x_{max} = Maximum Transverse Displacement for a Given Mode
θ_{max} = Maximum Rotational Displacement for a Given Mode
l_b = Beam Lever Arm

The relationship between torque and force will be referred to in this paper as the beam "lever arm". The required torque for an advanced actuator is the beam lever arm times the force used by the conventional actuator. An implicit assumption in the use of the beam lever arm is that each type of actuator is situated such that it removes the maximum possible amount of power from the vibrating beam. A force actuator is optimally located at the point of maximum transverse displacement, while a torque actuator is optimally located at the point of maximum rotation (Misovec, 1987). For example while the tip is a good location for force control of a mode 1 excitation, it is not a good location for control of a mode 2 excitation. These findings were verified by simulation (Misovec,1987). An effective force actuation scheme would require a number of actuators strategically placed along the beam. Analysis showed that a torque actuation scheme, on the other hand, would require only one torque actuator located at the tip (Misovec, 1987). Thus for this particular application, a torque actuation scheme has potential advantages over a conventional actuation scheme because it would require fewer actuators.

The beam lever arm is a strong function of mode. This is shown in Figure 2(a). This plot shows that at lower frequencies the torques that are required to give the same performance as conventional force actuators can be quite high (40 times the required force). By taking into account that at frequencies less 1 Hz, the force of the conventional actuators used for comparison is limited by stroke, the

'effective' lever arm is reduced. Figure 2(b) is a plot which shows the effect of limited stroke. Because the lowest frequency mode is the only mode with a frequency less than 1 Hz, limited stroke effectively reduces the beam lever arm for this mode.

As an estimate, 10 m will be used as a baseline effective beam lever arm. By multiplying this value by the maximum force capability of the conventional actuator (30 N see Table 2), SatCon actuators were designed to have a torque capability of approximately 300 N-m.

Actuator Stroke Sizing

Using the beam lever arm concept, a reaction mass torque actuator was sized for compatible performance with the baseline conventional reaction mass force actuator. The result of this analysis indicated that the required moment of inertia for the actuator would be unreasonably large for application to the beam model (Misovec,1987).

A CMG type actuator can be sized by considering Newton's Law which relates angular momentum (H), torque (τ), frequency (w) and angular stroke, (θ_s).

$$H = \tau / w \theta_s \qquad (2)$$

Because the actuator will be sized to give the same performance as the conventional actuators described previously, the torque used in this calculation is the force capability of the conventional actuator multiplied by the effective beam lever arm, which is a frequency dependent quantity. Thus, the required angular momentum is not a simple function of frequency. The required angular momentum is plotted versus angular stroke for the first three modes in Figure 3. A control moment gyro has large momentum storage capacities, and these values of angular momentum are reasonable. This plot was used to find the specifications for a small stroke and a large stroke actuator.

ACTUATOR CONCEPT SELECTION

Two baseline CMG type actuator designs were identified for comparison. One is a small stroke, high angular momentum design, and the other is a large stroke, low angular momentum design. The characteristics of these designs are presented below.

Table 3. Actuator Requirements

	STROKE	
	SMALL	LARGE
TORQUE (Nm)	300	300
MOMENTUM (Nms)	4000	400
STROKE		
(radians)	0.015	0.15
(degrees)	0.9	9

For the small stroke actuator, the air gap of the magnetic bearing (the clearance between the rotor and the stator) allows a sufficient angular stroke. Several small-stroke, magnetically-gimballed actuator

designs [Anderson, 1975; Sindlinger, 1977; Murakami, 1982] with gimbal angles up to about 2 degrees have been reported. For applications which require a larger stroke (greater than about 3 degrees), the length of the air gap which would be required causes the magnetic bearing design to be inefficient. The power required to establish the air-gap magnetic field is proportional to the square of the air-gap length. In addition, as the length of the air gap increases relative to other dimensions of the magnetic bearing, the amount of leakage flux also increases. Leakage flux is that flux which does not link the rotor and stator. It therefore does not contribute to the amount of force which is applied to the rotor and may even reduce it.

The large stroke actuator can be designed using a large-angle magnetic suspension (LAMS). A LAMS is a five-axes, actively-controlled magnetic bearing which is designed to accommodate relatively large angular motion of the rotor without an excessively long air gap. Actuation in the sixth degree of freedom can be provided by allowing the LAMS motor/generator to have gimballing capability.

Small-stroke Actuator

Flywheel.

Table 4 presents the characteristics for flywheels for the small-stroke actuator. A graphite/epoxy flywheel is compared to a high-strength steel flywheel. The mass of the composite flywheel is smaller than that of the steel flywheel by a factor of two and a half. The lower rotational speed of the steel flywheel results from its higher mass density. The advantage of the steel flywheel is that it may act as a portion of the magnetic circuit for the magnetic bearing.

Table 4. Flywheels for the Small-stroke Actuator

	COMPOSITE	STEEL
ASPECT RATIO	0.50	0.60
DIMENSIONS (cm)		
INNER DIAMETER	70	106
OUTER DIAMETER	35	64
AXIAL LENGTH	4	1.1
MASS (kg)	20	50
SPEED (krpm)	25	4

Small-gap Magnetic Bearings.

Figures 4(a) and 4(b) show the arrangement of eight magnets for flywheels which are either relatively large in diameter (an axial-air-gap magnetic bearing) or long (a radial-air-gap magnetic bearing). The figure also shows the lever arm (l) which relates bearing force (f) and torque (τ).

$$\tau = f \cdot l \tag{3}$$

A single expression relating the angular stroke (δ_{max}) to the air-

gap length (G) can be written.

$$G = \frac{1}{2} \sin(\delta_{max}) \tag{4}$$

This equation is used to determine the air-gap length from the dimensions of the flywheel and the angular stroke requirement.
The horseshoe-shaped core and coil which are shown in Figures 5(a) and 5(b) respectively were used to approximate the performance of a single magnetic bearing element [Anderson, 1975]. The design procedure is summarized here; more detail may be found in Misovec, 1987.

The air-gap area (A_g) is related to the force by the magnetic pressure (p_m). The magnetic pressure is determined from the flux density in the air gap (B_g).

$$f = p_m \cdot A_g \tag{5}$$

$$p_m = \frac{(B_g)^2}{2 \cdot \mu_o} \tag{6}$$

Magnetic pressure is typically low. For an air-gap flux density of 1 Tesla, the pressure is approximately 400 kPa (58 psi).

The magnet design procedure (Figure 5) is to give the core of the magnet a constant cross section which is equal to the area of the air gap. The poles of the magnetic core are assumed to have a length which is equal to that of the section thickness. The coil completely fills the available space. The volumes of iron and copper used for each magnetic bearing can be determined from these dimensions. Given the mass densities of the core material and the windings, the mass of each bearing is found by adding masses of these components. The total bearing mass is that of twelve bearing elements. The assumption is that eight bearing elements are required for torquing and an additional four are required to provide either radial or axial forces.

The current density (J) in the coil which is required to produce the air-gap magnetic field is determined from Ampere's law.

$$J \frac{A_g}{2} = \frac{2 B_g G}{\mu_o} \tag{7}$$

The power consumed by each bearing during torquing and the total power consumed by the bearing system (P_b and P_t) are then determined from the current density, the volume of a bearing coil (V_c), and the conductivity of the material (σ).

$$P_b = \frac{J^2 V_c}{\sigma} \tag{8}$$

$$P_t = 4\ P_b \qquad (9)$$

Table 5 contains the performance data for magnetic bearing elements for use with the flywheels from Table 4. A baseline power consumption during torquing of 100 W was assumed.

Table 5. Magnetic Bearings for the Small-stroke Actuator

	COMPOSITE	STEEL
FLUX DENSITY (T)	1.0	0.6
AIR-GAP LENGTH (cm)	4.0	0.6
CURRENT DENSITY (MA/m^2)	4.4	3.4
BEARING ELEMENT MASS (kg)	2.2	3.5
TOTAL BEARING MASS (kg)	26.4	42.0

Small-stroke Actuator Summary.

Table 6 summarizes the performance of the two alternatives which were considered for the small-stroke actuator. Although the mass of the actuator which employs a steel flywheel is twice that of one which employs a graphite/epoxy flywheel, this might be a viable candidate for a laboratory-scale demonstration. The advantage of the steel flywheel is that it may act as part of the magnetic circuit for the bearing.

Table 6. Small-stroke Actuator Performance

FLYWHEEL TYPE	Gr/ep	STEEL
MASSES (kg)		
FLYWHEEL	20	50
BEARING SYSTEM	26	42
TOTAL	46	92
POWER (W)	100	100

Large-stroke Actuator

Several types of actuators using large angle magnetic suspensions (LAMS) were examined. The conventional technology LAMS studied for this actuator application include two types of attraction force LAMS as well as a Lorentz force LAMS. In addition, a LAMS using superconducting technology was also studied.

Conventional-technology LAMS.

Flywheel.

The angular momentum storage capacity which is required for the large-stroke actuator is one tenth that of the small-stroke actuator. For both of the conventional technology LAMS concepts which are considered in this analysis, the rotating magnetic components will

C-4

store sufficient angular momentum for this actuator.

Conventional LAMS Torque Actuation Requirements

In addition to free rotation about the spin axis (SA), a LAMS provides controlled (but limited) angular motion about each of the orthogonal lateral axes. A reference frame based on the spherical coordinates shown in Figure 6 is employed for analysis.

A LAMS be analyzed in terms of forces that are spherically radial (f_R), azimuthal (f_α), elevational (f_β), or some combination of these as is shown in Figure 6. At the k^{th} point of force application, which is located at position (R_k,α_k,β_k), the net torque resolved in orthogonal coordinates is as follows.

$$\begin{aligned} \tau_k = {} & R_k(-f_{\alpha k}\cos\alpha_k\sin\beta_k + f_{\beta k}\sin\alpha_k)\, u_x \\ & - R_k(f_{\alpha k}\sin\alpha_k\sin\beta_k + f_{\beta k}\cos\alpha_k)\, u_y \\ & + R_k f_{\alpha k}\cos\beta_k\, u_z \end{aligned} \tag{10}$$

To meet the control torque requirements, the forces at each of N_1 points must satisfy the following.

$$\tau_x = \sum_{k=1}^{N_1} R_k(-f_{\alpha k}\cos\alpha_k\sin\beta_k + f_{\beta k}\sin\alpha_k) \tag{11}$$

$$\tau_y = \sum_{k=1}^{N_1} -R_k(f_{\alpha k}\sin\alpha_k\sin\beta_k + f_{\beta k}\cos\alpha_k) \tag{12}$$

$$0 = \sum_{k=1}^{N_1} R_k f_{\alpha k}\cos\beta_k \tag{13}$$

Equation (13) precludes first order interaction between the LAMS and the drive. Similar equations can be derived for LAMS actuation forces [Downer, 1986].

Examination of Equations (11) through (13) provides some insights into possible ways to design a LAMS. The simplest way to satisfy the "no-SA-torque" requirement (Equation (13)) is to not employ forces that act in the azimuthal direction ($f_{\alpha k} = 0$, for all k). With this constraint satisfied, it becomes clear that, for torquing, elevational forces alone will be a satisfactory configuration. The following two sections illustrate how elevational forces and thus control torques can be obtained in the LAMS systems analyzed in this study.

Attraction Force LAMS Designs

In order to use an attraction-force magnetic bearing in a large-angle configuration, the attractive surfaces on the rotor and stator are shaped to approximate concentric spheres. Figure 7 shows the forces exerted by one pole of an attraction-force LAMS that employs both primary and secondary attraction forces. The primary force acts in a direction that is spherically radial, while the secondary force

acts in the elevational direction. If the nominal air-gap length (G_o) is small in comparison to other dimensions, the forces may be approximated by assuming that the interacting surfaces are nearly parallel flat plates. The elevational attraction-force is readily evaluated for a spherical geometry.

$$f_{\beta k} = c_{a\beta} B_{gk}^2 \tag{14}$$

where $c_{a\beta}$ is a geometrical constant and B_{gk} is the flux density in air gap.

The components of the torque vector that is applied to the rotor by the k^{th} pole are found by substituting Equation (14) into Equations (11) and (12).

$$\tau_{xk} = R_o c_{a\beta} \sin\alpha_k B_{gk}^2 \tag{15}$$

$$\tau_{yk} = R_o c_{a\beta} \cos\alpha_k B_{gk}^2 \tag{16}$$

where R_o is the nominal spherical radius.

The two attraction-force LAMS designs are biased electro-magnets. Both employ two wound, four-pole disks on the stator. A magnetic field is maintained in the air gap when no mechanical load is present. The LAMS designs, however, differ in the manner through which the magnetic field is produced. The LAMS design which is shown in Figure 8(a) employs a heteropolar field maintained by current in control coils wound on salient poles. The second design alternative (Figure 8(b)) utilizes a permanent magnet to produce a homopolar bias field. The permanent magnet is shown as a part of the rotor, but it could also be incorporated in the stator structure if stresses due to rotation are a concern. A more complete description may be found in Downer, 1986.

Lorentz Force LAMS Designs

The Lorentz-force LAMS design (Figure 9(a)) consists of two identical magnetic structures each containing a rotor and a stator. Each rotor contains an axially-oriented, permanent magnet and sufficient core material to yield an approximately spherically-radial magnetic field in the air gap.

$$B = B_g u_R \tag{17}$$

Each stator consists of a thin shell containing four control coils as is shown in Figure 9(b). The figure also shows the direction for positive current.

The elevational force density vector at a point (R_k, α_k, β_k) within the k^{th} coil is the cross product of the coil current and flux density vectors.

$$\rho_{fk} = J_k \times B = B_g J_{\alpha k} u_\beta \tag{18}$$

The net elevational force (f_k) exerted on the rotor by the k^{th} coil is found by integrating the negative of the force density over the fraction of the active region which contains wire.

The net torque vector (τ_k) and its Cartesian components (τ_{Xk}, τ_{Yk}) are found by integrating the moment of the force density over the active region. The complete analysis may be found in Downer, 1986.

Comparison of Conventional LAMS

Figure 10(a) shows that, for a fixed range of LAMS mass, the power consumption of a Lorentz-force LAMS is lower than that of either of the attraction-force suspensions. The power consumption of a heteropolar, attraction-force LAMS is nearly four times that of a PM-field, Lorentz-force LAMS with the same mass. The power consumption of a homopolar LAMS is 30-50% higher than for a Lorentz-force LAMS (Downer, 1986).

Figure 10(b) shows the increased mass of the two attraction-force LAMS design options over the Lorentz-force LAMS for a range of control-torque power consumption. For power consumption that is equal to that of a Lorentz-force LAMS, a heteropolar LAMS must have a mass that is between two and a half and three times that of the Lorentz-force LAMS. The mass of a homopolar LAMS is not as great; in the range of 25-50% more than that of a Lorentz-force LAMS with equal power consumption (Downer, 1986). A baseline Lorentz force LAMS actuator for this application would mass 100 kg and require 400 W of power.

Superconducting LAMS.

The superconducting LAMS, as its name suggests, employs a superconducting coil for the elimination of all conventional magnetic structures in order to produce an energy-efficient, light-weight design. Figure 11 is a partially cut-away view which shows the rotating components (superconducting coil and flywheel) and cryogenic housing of a two-degree-of-freedom CMG which employs a superconducting LAMS. The superconducting coil is a solenoid which operates in persistent-current mode (without an electrical input). The current in the solenoid persists because of the lack of resistance in the superconducting material. The spherical case which surrounds the rotating components also serves as the cryostat for the superconducting solenoid.

A high-strength graphite/epoxy composite flywheel is attached to the solenoid to provide angular momentum storage capacity. The outer diameter of the flywheel is machined to a spherical shape. This allows the flywheel to be completely gimballed without contact with the case.

The normal coils shown in Figure 12 are used to apply torques to the flywheel. The figure illustrates the torquing mechanism. Assuming that the spin axis is along the z-axis, the magnetic field (B), produced by the superconducting solenoid at the location of the torquing coils is approximately parallel to the z-axis and constant. The torque (τ) results from the interaction of the dipole moment (μ) produced by the current (I) in the normal coil and the magnetic field.

In order to estimate the performance of a superconducting LAMS, a

set of scaling laws have been developed to scale from the a 34,000 Nm design to a 300 Nm design appropriate for flexible structure control of the beam model (Misovec,1987). Table 7 presents the results obtained by scaling the performance of the high-torque LAMS described in Downer (1987) to a size appropriate to the present application. Eight additional normal coils are used in order to apply radial and axial forces on the rotor. Each of the other eight coils required for the LAMS is assumed to have a mass which is equal to that of a torquing coil.

Table 7. Performance of Superconducting LAMS

	CURRENT APPLICATION
TORQUE (Nm)	300
ANG. MOM. (Nms)	400
MASSES (kg)	
SOLENOID	33
TORQUE COILS (4)	16
OTHER COILS (8)	32
TOTAL	81
POWER (W)	380

There is room for optimization of the design to reduce the power consumption of the torquing coils at the expense of added coil mass.

Comparison of Actuator Designs

Both conventional-technology and superconducting LAMS were also shown to be feasible for flexible structure control although the mass of the LAMS designs are higher than the mass of the small stroke designs. For future large space structure actuator development, the LAMS is preferred over the small stroke approach because of its larger momentum transfer capability. The added momentum transfer allows the large stroke actuator to be used in a variety of systems applications where high frequency control of flexible structure vibrations combined with significant low frequency momentum storage for slewing or attitude control are required.

Although the superconducting LAMS is 20% lower in mass than the conventional LAMS, this difference is not significant as there is room for optimization in both designs. The difference becomes less significant as the torque capability of the actuator is reduced. A superconducting LAMS may be the best choice actuator for specific applications where high torques are required. In addition, the superconducting LAMS is a high risk development project. On the other hand, for a modest development cost, the conventional-technology LAMS actuator can have a wider range of applications.

Thus a conventional-technology LAMS, either attraction force or Lorentz force is recommended for further development for flexible structure control.

CONTROLLER DESIGN

The closed-loop performance of both the conventional and advanced actuators were analytically obtained on the baseline flexible beam model using full-state, linear-quadratic-optimal feedback. These closed-loop simulations were primarily used to validate the open-loop comparison of actuator force versus torque control effectiveness. The controller designs were done using linear quadratic design tools (Kwakernaak and Sivan, 1972), which are based on the minimization of a quadratic cost functional.

The force/torque tradeoff derived previously is verified here by simulations of a beam vibrating in mode 1. A controller, which used tip force actuation was designed to give a peak control force level of 1.1 N; this is the stroke-limited level of force of the conventional actuator. Then the level of damping for this mode was computed. Then a controller, using tip torque actuation, was designed to give the same level of damping performance. The peak force should be the beam lever arm for mode 1 (40 m) multiplied by 1.1 N (or equivalently, the effective beam lever arm multiplied by 30 N). Figure 13 shows the results of this analysis. The peak torque which must be used to achieve the same performance as the force actuator is approximately 45 Nm. These plots indicate that the beam lever arm concept was verified for closed loop control of mode 1.

CONCLUSIONS

This research has investigated the feasibility of advanced six-degree-of-freedom actuators employing magnetic suspensions for use in actively controlling large space structures. These advanced actuators consist of a magnetically suspended mass that has three-degrees-of-freedom in both translation and rotation. These torque and force producing actuators can be used in a similar manner to conventional linear reaction mass actuators to control spacecraft vibrations.

The major advantages of these advanced actuators include high bandwidth compared to conventional control moment gyros (CMG's) and both large momentum storage capability and multi-degree-of-freedom actuation compared to conventional linear reaction mass actuators. The combination of high bandwidth and large momentum storage allow these advanced actuators to be used in applications, such as space robotic arms, that have both slewing and vibration requirements. Other similar applications include the combined control of the attitude and flexible structure dynamics of small spacecraft with flexible appendages. Because of their six-degree-of-freedom actuation characteristics and torquing abilities, these advanced actuators were shown to be capable of replacing numerous linear reaction mass actuators.

Design definitions of four actuators were developed, two with small angular strokes (approximately 1 degree) and two with large angular strokes (approximately 10 degrees). Simple models of these actuators were developed that allowed first-order comparisons of their mass and power. The performance goal was to have equivalent control effectiveness of low frequency modes as a conventional, commercially

available linear reaction mass actuator. Of the advanced actuators, the large angle magnetic suspensions were best with the non-optimized designs massing about 100 kg for equivalent low frequency control effectiveness in two directions.

The key technology development required for these advanced actuators is the large-angle-magnetic suspensions and associated controllers.

REFERENCES

1. Anderson, W. and N. Groom, The Annular Momentum Control (AMCD) Device and Potential Applications, NASA TN-D 7866, 1975.

2. Davis, L., D. Hyland, T. Otten, and F. Ham, "Mast Flight System Dynamic Performance," First NASA/DOD CSI Technology Conference, Norfolk, Virginia, November 1986.

3. Downer, J. Design of Large-angle, Magnetic Suspensions, ScD Thesis, Massachusetts Institute of Technology, May 1986.

4. Downer, J., D. Eisenhaure, R. Hockney, and B. Johnson, "Applications of Magnetic Bearings to High-Torque, Satellite Attitude Control Wheels," Proceedings of the Twenty-second Intersociety Energy Conversion Engineering Conference, Philadelphia, PA, August 1987.

5. Downer, J., Hockney, R., Johnson, B., Misovec, K. " Advanced Actuators for the Control of Large Space Structures, " Final Report for NASA Grant NAS1-18426, SatCon Technology Corporation, R07-87, August, 1987.

6. Kwakernaak, Huibert, and Raphael Sivan, Linear Optimal Control Systems, Wiley-Interscience, New York, 1972.

7. Murakami, C., "Development Activities on Magnetic Bearings for Space Use in National Aerospace Laboratory of Japan," Proceedings of the Sixth International Workshop on Rare Earth Cobalt Permanent Magnets and Applications, Technical University of Vienna, August--September 1982.

8. Sindlinger, R. "Magnetic Bearing Momentum Wheels with Magnetic Gimballing Capability for 3-Axis Active Attitude Control and Energy Storage," Conference on Attitude and Orbit Control Systems, ESA SP-128, Noordwijk, November 1977.

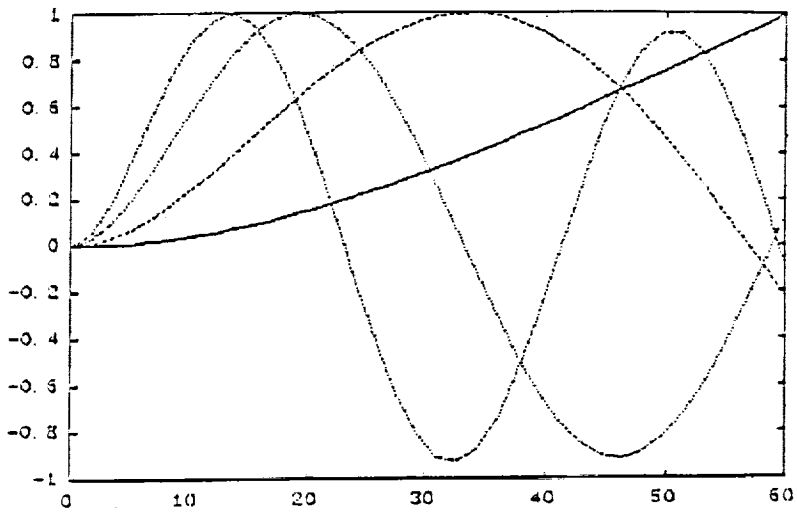

Figure 1. Mode Shapes

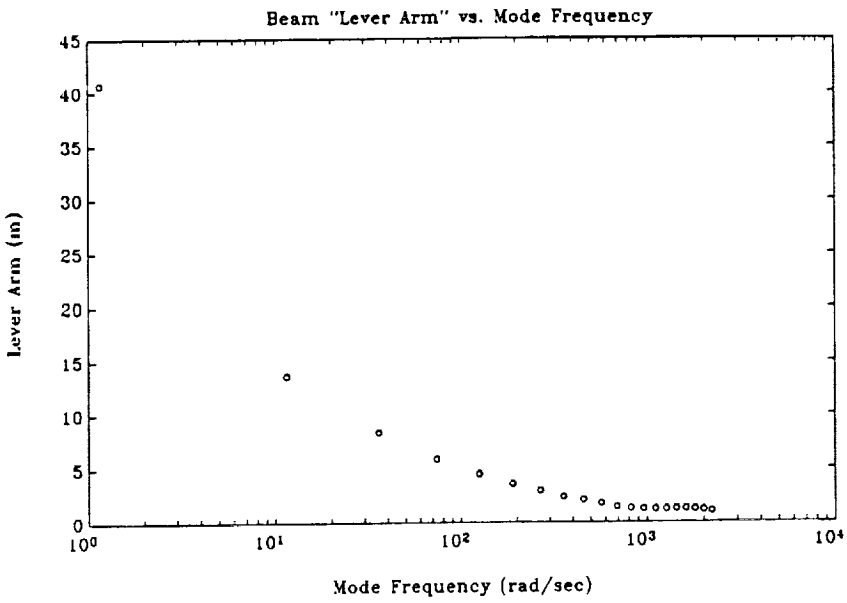

(a) Beam Lever Arm

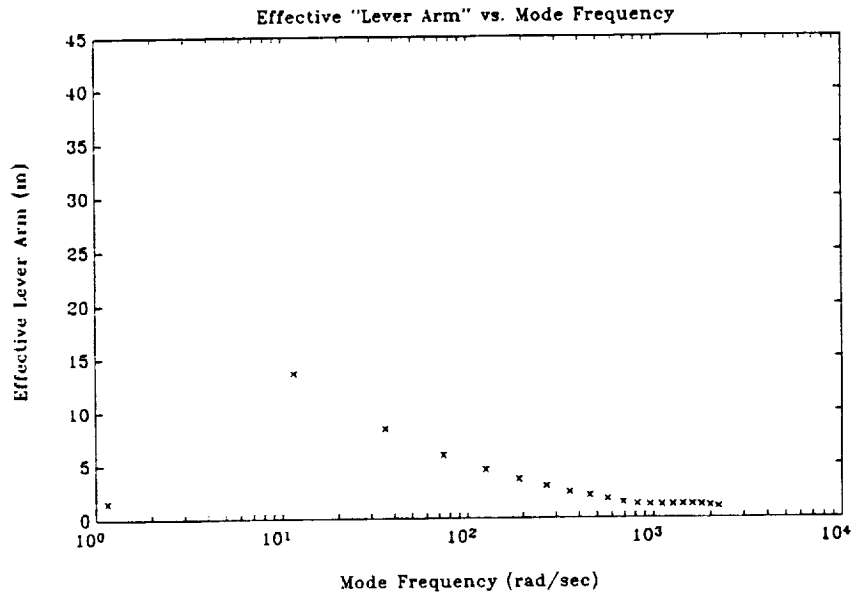

(b) Effective Beam Lever Arm

Figure 2.

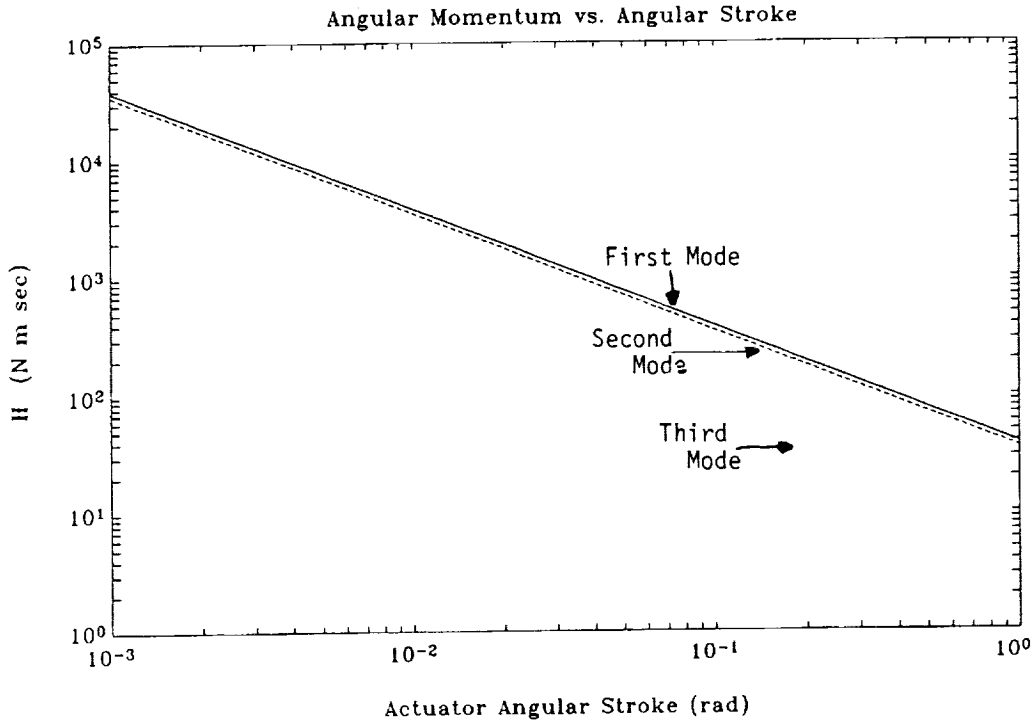

Figure 3. Required Angular Momentum vs Angular Stroke CMG Neglecting Effect of Beam Vibrations

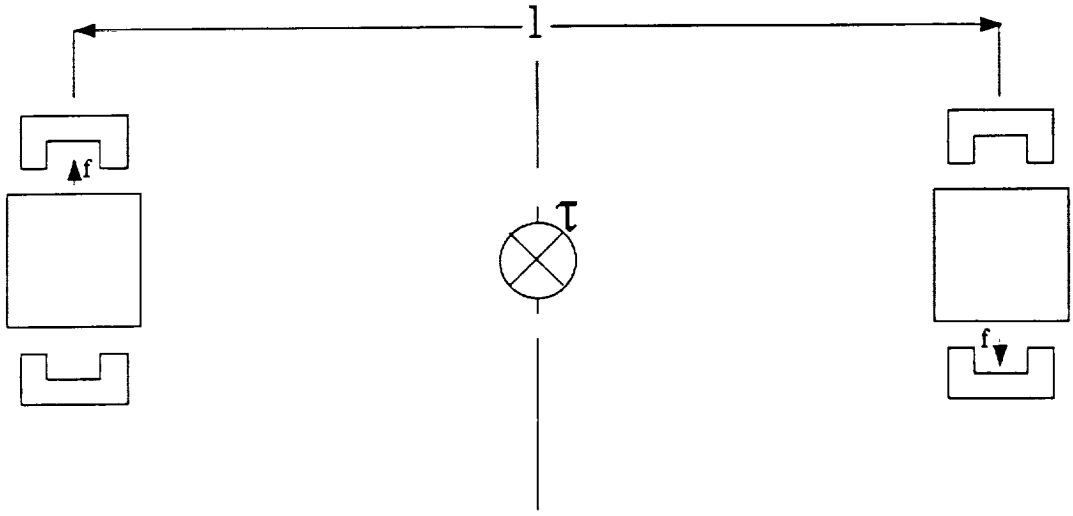

(a) Long Flywheels

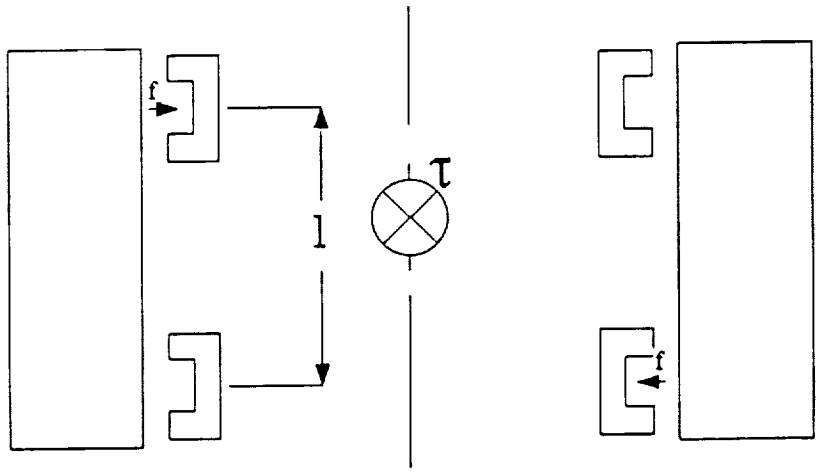

(b) Large-diameter Flywheels

Figure 4. Magnetic Bearing Configuration

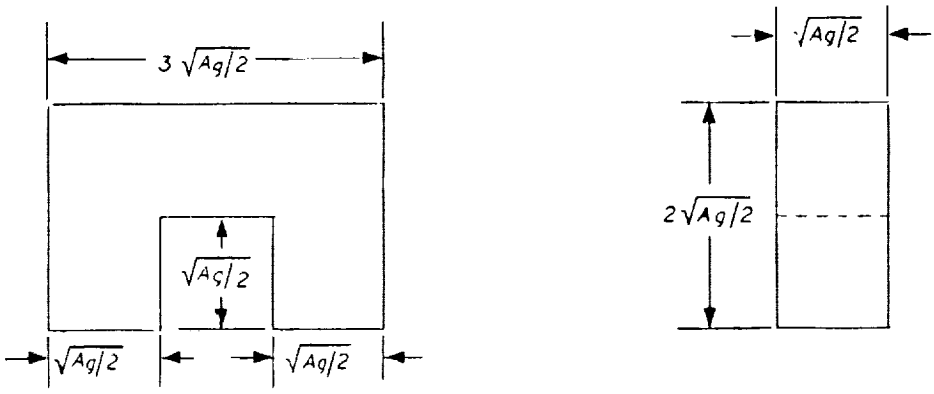

(a) Horseshoe Magnet Core

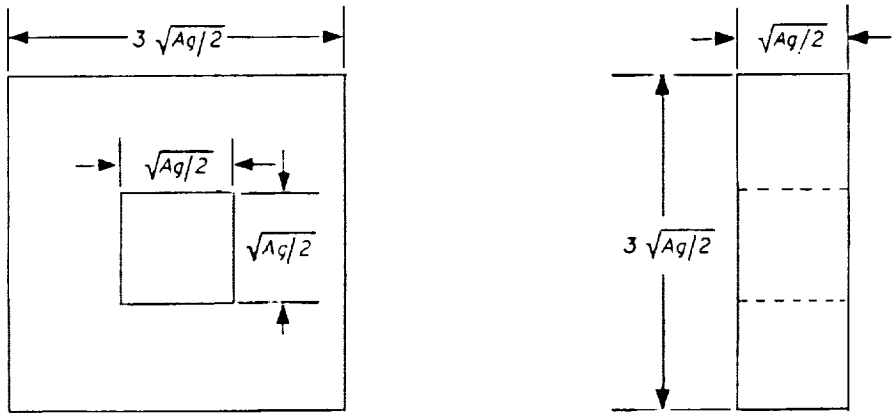

(b) Horseshoe Magnet Coil

Figure 5. Magnet Design

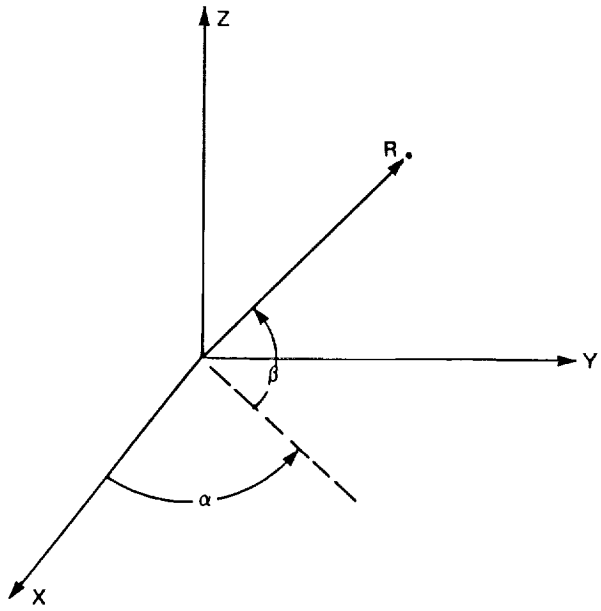

(a) Spherical Coordinate System

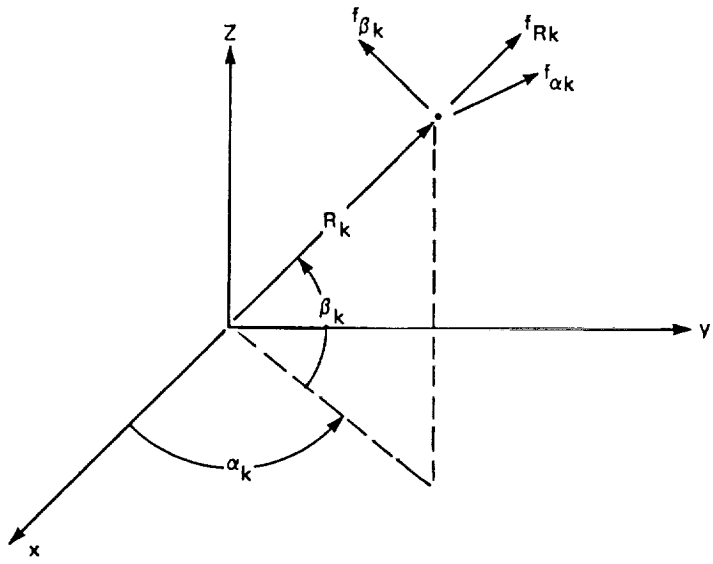

(b) LAMS Force Components

Figure 6. Geometric Symmetry Considerations for a LAMS

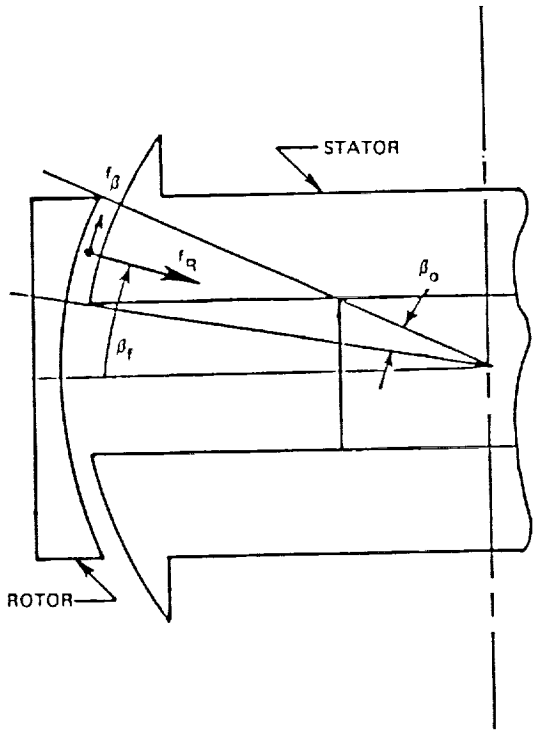

Figure 7. Forces in an Attraction-force LAMS

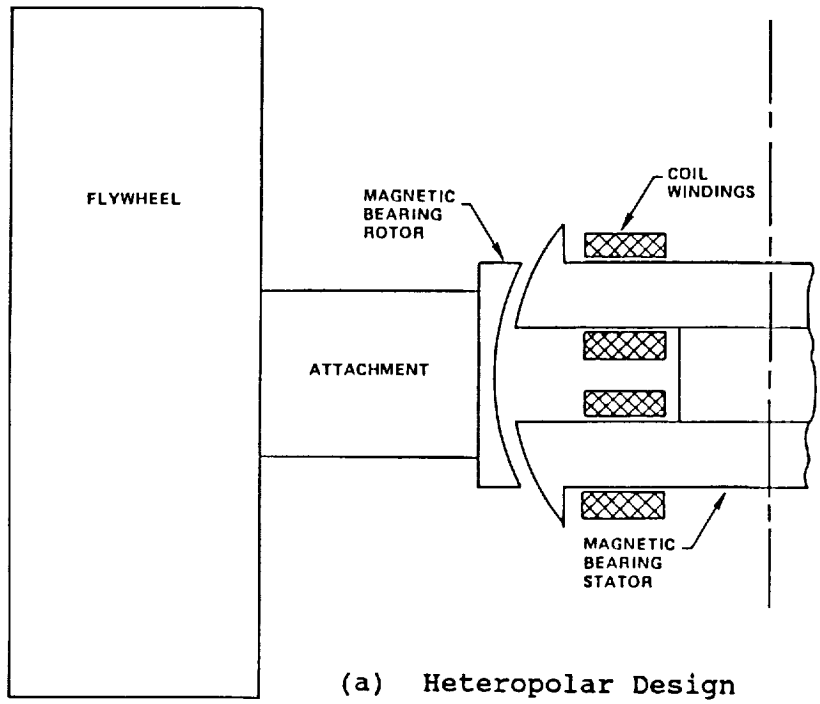

(a) Heteropolar Design

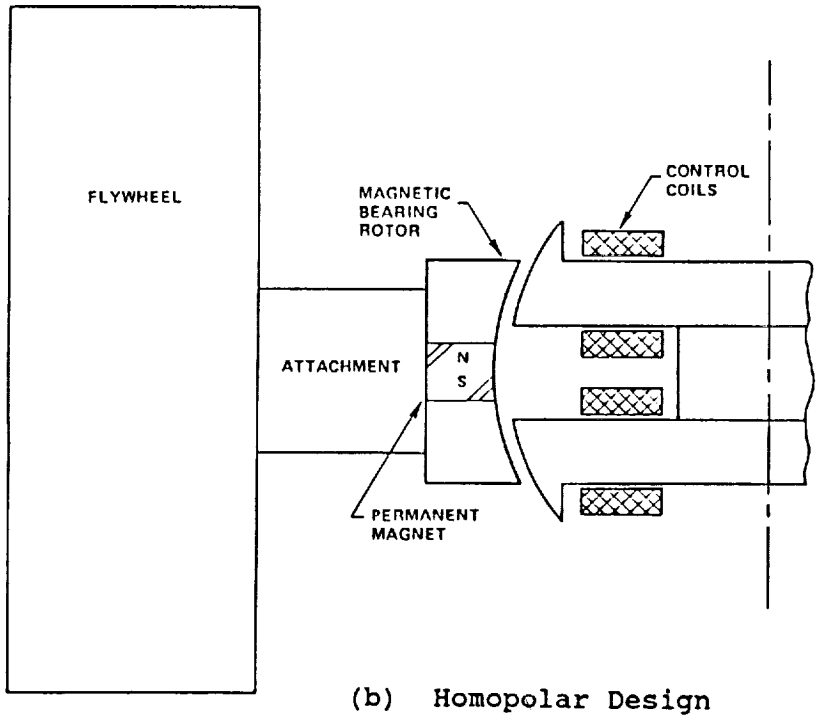

(b) Homopolar Design

Figure 8. Attraction-force MAMS Design Options

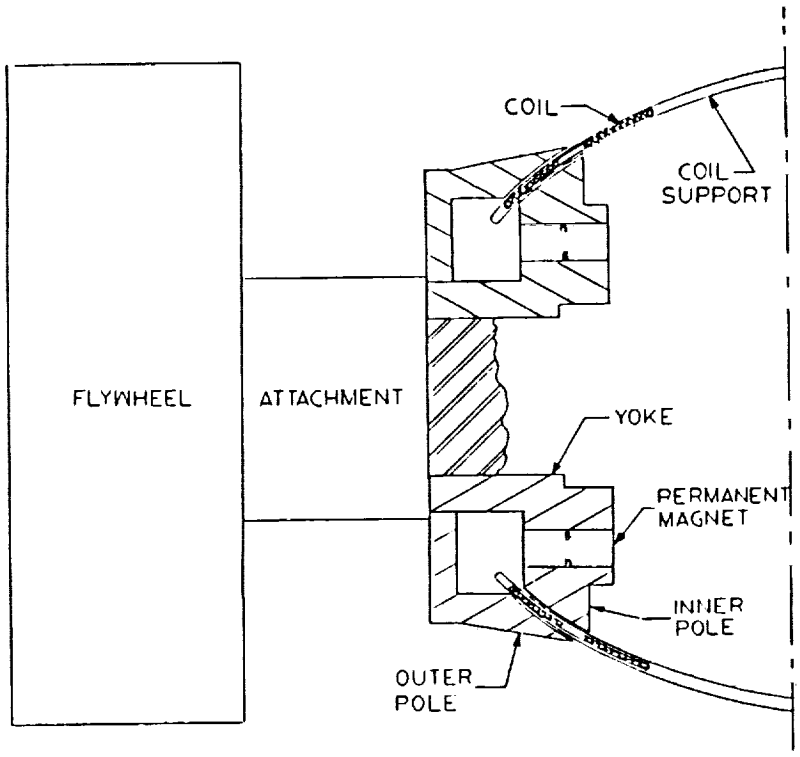

(a) Section View

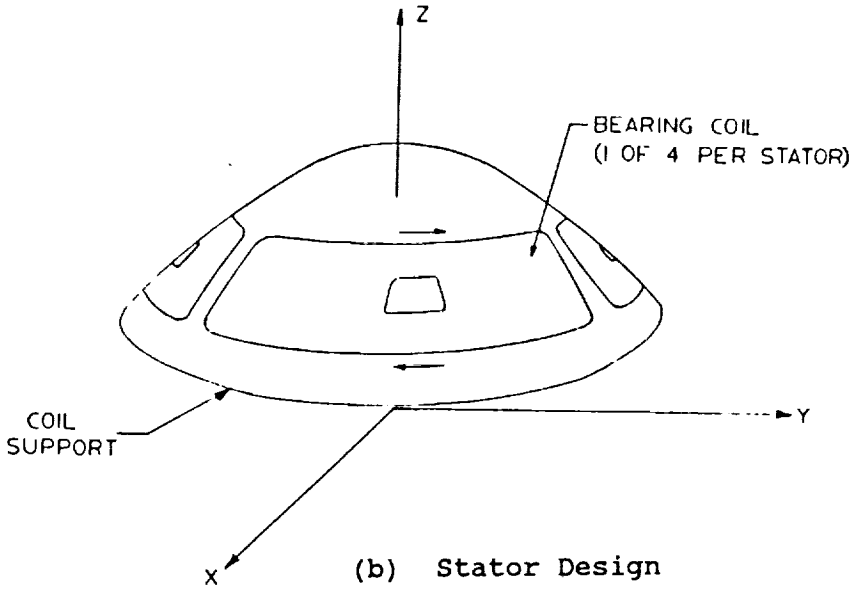

(b) Stator Design

Figure 9. Lorentz-force LAMS Design Option

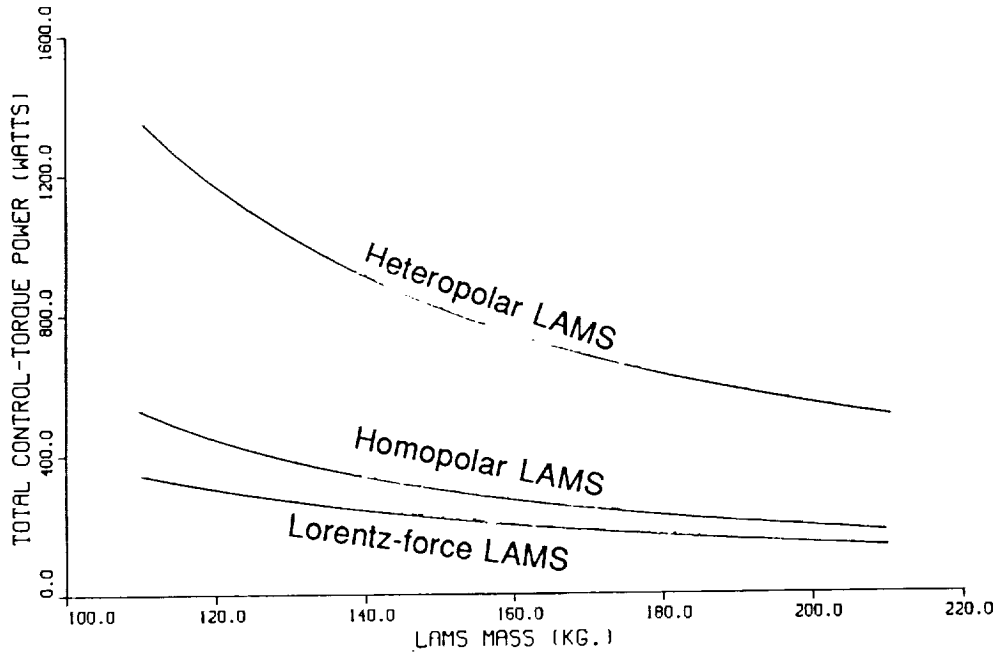

(a) **Fixed Mass**

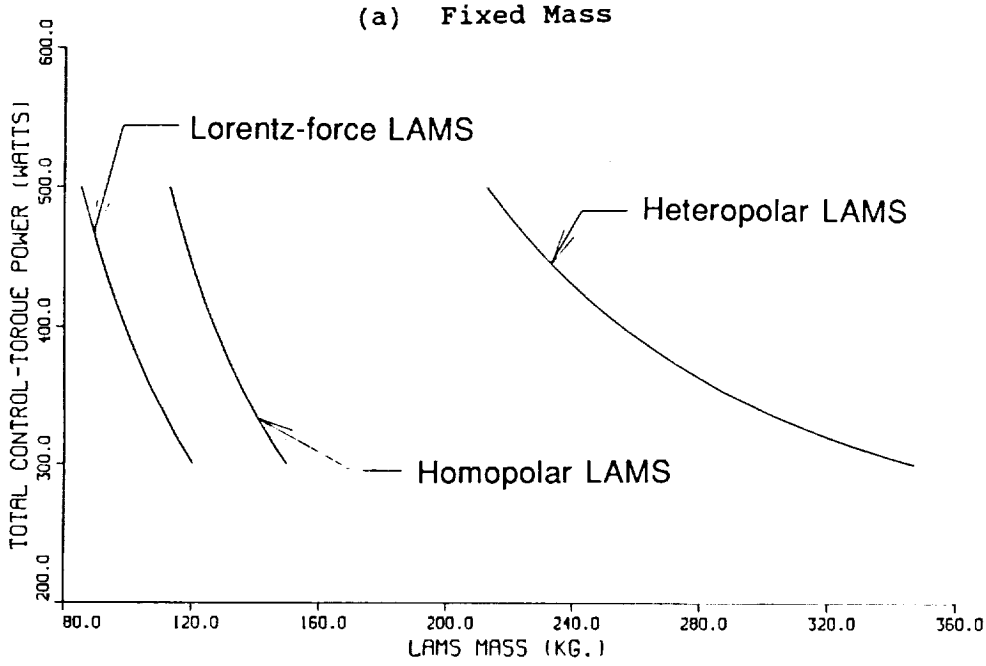

(b) **Fixed Power**

Figure 10. LAMS Trade-off Comparison

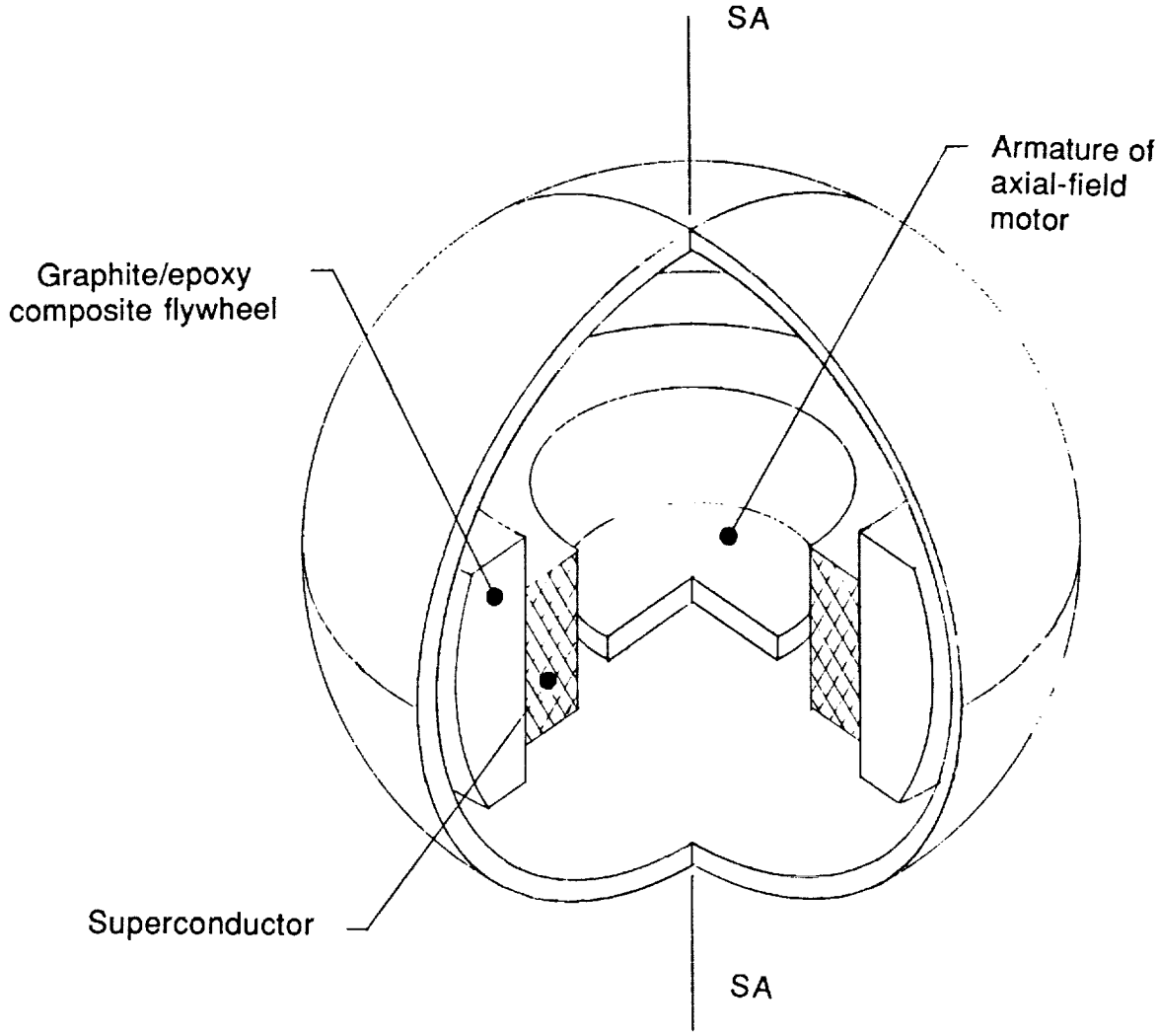

Figure 11. Superconducting CMG

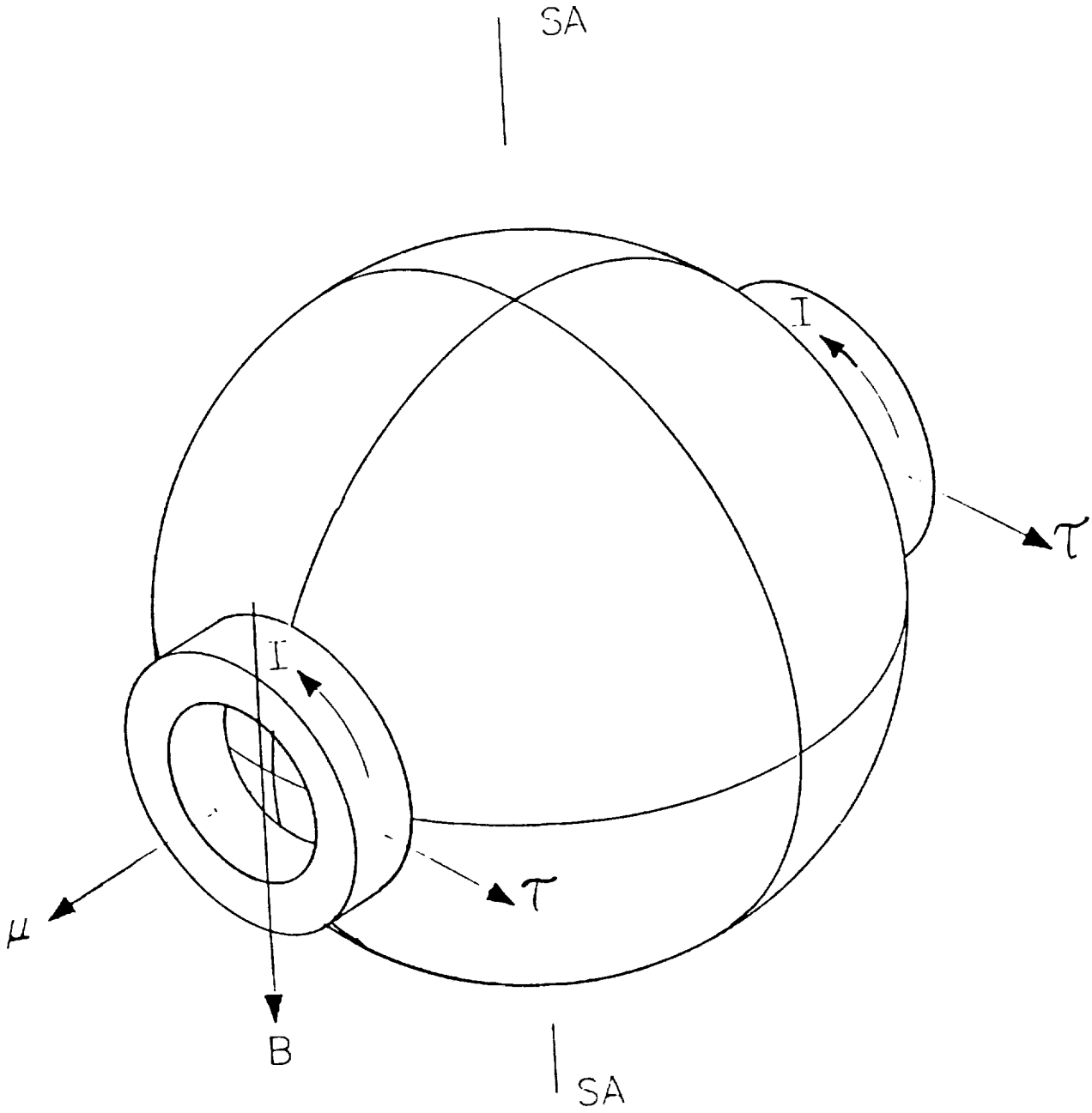

Figure 12. Torque Operation

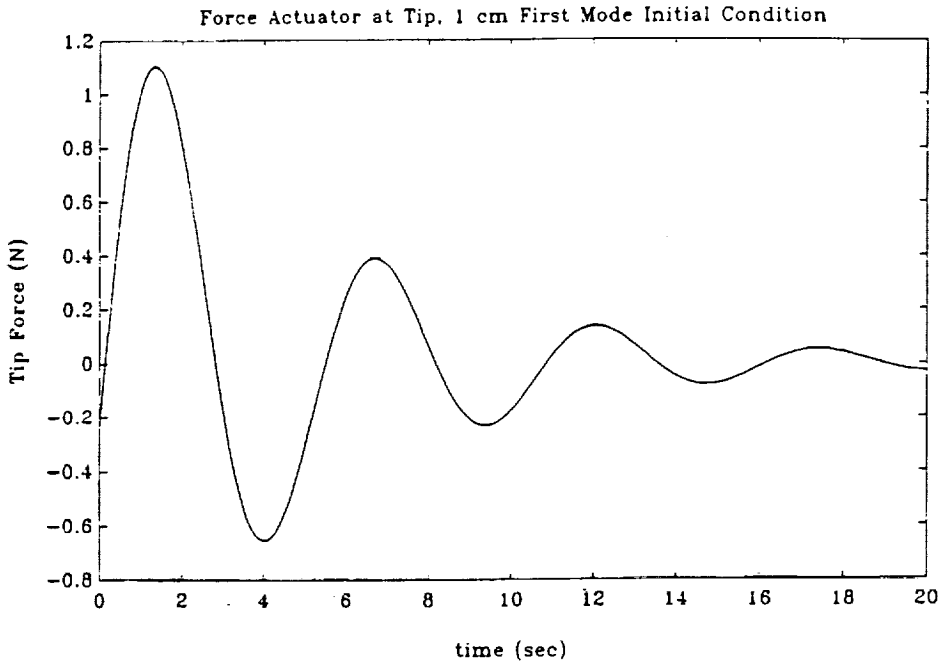

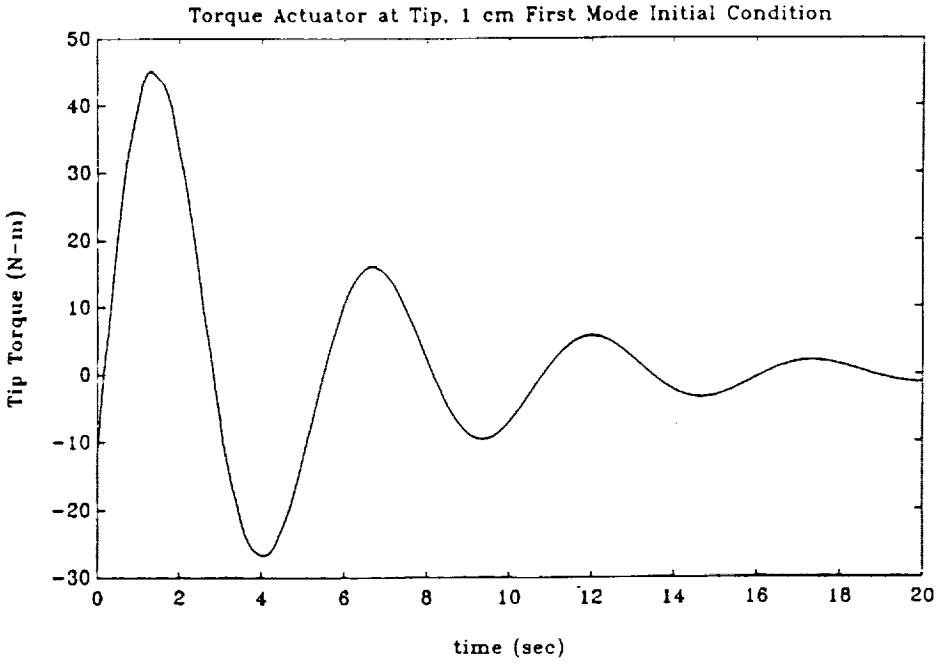

Figure 13. Beam Lever Arm Verification for Mode 1